Coordination Chemistry

DOI: 10.1002/ange.201103233

Bioinspired Five-Coordinate Iron(III) Complexes for Stabilization of Phenoxyl Radicals**

*Marco M. Allard, Jason A. Sonk, Mary Jane Heeg, Bruce R. McGarvey, H. Bernhard Schlegel, and Cláudio N. Verani**

Dedicated to Professor Karl Wieghardt

Considerable effort has been directed towards the integration of biomimetic principles into molecular materials that have customized and controllable properties.[1] The notion of stimulus-triggered molecular switching between two or more ground states of comparable energy[1a,2] is particularly relevant because such switching leads to detectable electronic and structural changes. Coordination complexes that merge transition-metal ions with ligands that stabilize organic radicals are among the most promising candidates for redox-responsive switching processes. Among the electroactive ligands that have been well characterized, those that contain phenolate moieties are significant because of their synthetic versatility and redox accessibility. This importance has been highlighted by studies on metal–phenoxyl complexes that have several geometries.[3] Iron(III) complexes that contain phenolates tend to favor an octahedral geometry and are electrochemically reversible, but usually do not withstand multiple redox cycles. Thus, an understanding of the alternative geometries of such complexes becomes a necessary strategy for the future development of redox switches.

We are investigating bioinspired designs that incorporate the basic geometries that are present in redox-versatile enzymes, such as tyrosine hydroxylase[4] and intradiol dioxygenase,[5] in which five-coordinate iron(III) centers support radical-based mechanisms for generating L-3,4-dihydroxyphenylalanine (L-DOPA) and cleaving catechol-type rings, respectively.

We have reported the behavior of high-spin iron(III) complexes that are confined to low-symmetry, pentadentate N_2O_3 environments.[6] In these complexes, the assignment of oxidation states[7] becomes challenging because of the contributions of ligand- and metal-centered orbitals to the same redox process, and the presence of five unpaired electrons. Nonetheless, we have shown that high oxidation states are unavailable to the metal ion, and that the ligand supports up to three consecutive oxidations, which leads to antiferromagnetic interactions. Relative to octahedral fields, these five-coordinate environments are expected to yield low-degeneracy molecular orbitals (MOs) that are sensitive to subtle but noticeable structural changes in the ligands. These changes should lead to orbital rearrangements that modify the sequence by which phenolate oxidations occur.

Herein, we investigate the behavior of the five-coordinate species $[Fe^{III}L^1]$ (**1**) and $[Fe^{III}L^2]$ (**2**, Scheme 1), in which a low-symmetry ligand field is purposefully enforced around the $3d^5$ metal ion by the N_2O_3 ligands. Ligands $[L^1]^{3-}$ and $[L^2]^{3-}$ both contain N_2O_3 environments with three phenolate moieties, denoted A, A′, and B; phenolates A and A′ share the same amine group and are chemically equivalent, whereas phenolate B is attached to either an azomethine group in L^1 or to a methylamine group in L^2. Both species have four accessible ground states: $[Fe^{III}L]^0/[Fe^{II}L]^-$, $[Fe^{III}L^{\bullet}]^+$, $[Fe^{III}L^{\bullet\bullet}]^{2+}$, and $[Fe^{III}L^{\bullet\bullet\bullet}]^{3+}$. The aim of this study is to determine the sequence in which each of the phenolate rings is oxidized in the presence of the azomethine and the methylamine groups, and to test the feasibility of consecutive, multielectronic oxidations by ion-pairing effects with the supporting electrolyte. This study is intended to contribute to the fundamental understanding of the redox and electronic behavior of high-spin $3d^5$ ions in five-coordinate ligand fields, and provide significant insight into bioinspired redox cycling.

Complexes **1** and **2** were synthesized as previously described[6b,c] and crystals that were suitable for analysis by

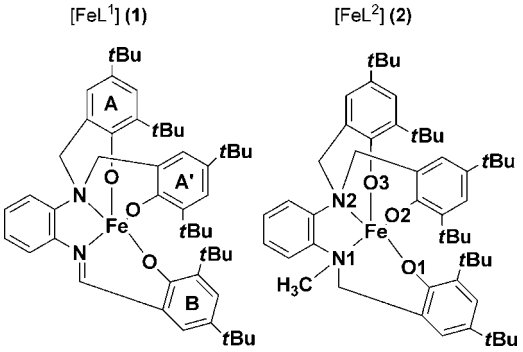

Scheme 1. Five-coordinate iron(III) complexes **1** and **2**.

[*] M. M. Allard, J. A. Sonk, Dr. M. J. Heeg, Prof. H. B. Schlegel, Prof. C. N. Verani
Department of Chemistry, Wayne State University
5101 Cass Ave. Detroit, MI 48202 (USA)
E-mail: cnverani@chem.wayne.edu
Homepage: http://chem.wayne.edu/veranigroup/
B. R. McGarvey
Department of Chemistry and Biochemistry
University of Windsor, Windsor, Ontario N9B 3P4 (Canada)

[**] This work was funded by the National Science Foundation through grants CHE-0718470 and CHE-1012413 to C.N.V. and CHE-0718470 to H.B.S. Partial support from the Department of Energy (DE-FG02-09ER16120) is also acknowledged. Dr. Richard L. Lord is acknowledged for critical discussions.

Supporting information for this article is available on the WWW under http://dx.doi.org/10.1002/anie.201103233.

X-ray diffraction were obtained. Both complexes crystallized with five-coordinate, high-spin iron(III) centers that are surrounded by fully deprotonated ligands to yield the neutral species (Table S1 and S2 in the Supporting Information). The bond lengths and angles were consistent with other examples in the literature.[3c,g,i, 6b,c] The ORTEP diagrams with selected bond lengths and angles for **1** and **2** are shown in Figure 1.

The structure of **1** has a short C=N azomethine bond between the C7 and N1 atoms of the 2,4-di-*tert*-butyl-6-methylphenol moiety. In contrast, **2** has a methyl group appended to the N7 atom, and is thus a tertiary amine that cannot form an azomethine. The other bonds in **1** and **2** are comparable in length, although some differences are noted in the distorted trigonal-bipyramidal environments, with $\tau =$ 0.54 and 0.66, respectively.[6b] Iron(III) phenolate species have complex electrochemical behavior,[3e, 6b,c, 8]; therefore, the redox responses for **1** and **2** were studied in CH_2Cl_2 with either $TBAClO_4$ or $TBAPF_6$ (TBA = tetrabutylammonium) as supporting electrolytes. In all cases, $TBAClO_4$ lowers the redox potentials and the Fe^{III}/Fe^{II} couple appears between −1.48 V and −1.55 V versus Fc^+/Fc (Table S3 in the Supporting Information). The ligand-centered redox processes were found to be susceptible to the nature of the supporting electrolyte (Figure 2). In the presence of $TBAClO_4$, there is a single anodic wave at 0.63 V ($\Delta E_p = 0.16$ V) for **1**. The amplitude and potential of this wave suggest a two-electron, ligand-centered redox process, when internally compared to the Fe^{III}/Fe^{II} couple. In the presence of $TBAPF_6$, the wave for the same process unfolds slightly into two independent, one-electron processes at 0.55 V ($\Delta E_p = 0.15$ V) and 0.73 V ($\Delta E_p = 0.16$ V) versus Fc^+/Fc. Interestingly, the third expected ligand-centered redox process for **1** was not detected under these conditions. Remarkably, in the presence of $TBAPF_6$, **2** has two well-separated peaks for one-electron redox processes that are centered at 0.48 V (ΔE_p 0.12 V) and 0.75 V ($\Delta E_p = 0.12$ V) versus Fc^+/Fc, and a subsequent irreversible anodic process at $E_{pa} = 1.09$ V versus Fc^+/Fc. These redox processes are consistent with the oxidation of all the three phenolate groups into phenoxyl radicals. On the other hand, when $TBAClO_4$ is used in conjunction with **2**, a redox process is detected at 0.63 V ($\Delta E_p = 0.16$ V), which can be attributed to a two-electron process based on its relative amplitude. This behavior suggests that sequential, one-electron redox processes occur for **1** and **2** in $TBAPF_6$, whereas $TBAClO_4$ supports multielectronic redox processes. Although this ion-pairing phenomenon has been described by Lintvedt and Kramer as well as[9] Geiger et al.,[10] it is seldom detected in coordination complexes. Species **1** and **2** have a remarkable cyclability with both supporting electrolytes. These species withstand well over 30 redox cycles at 150 mV s^{-1} without noticeable decomposition.

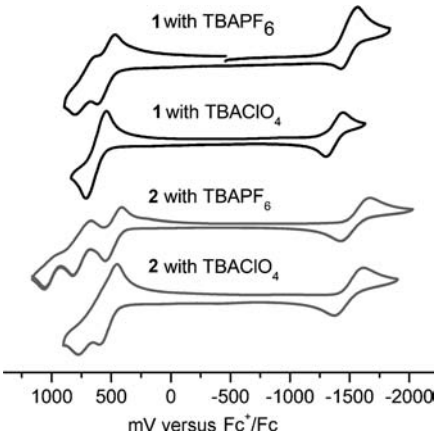

Figure 2. Cyclic voltamograms for complexes **1** and **2**. Fc^+/Fc = ferrocenium/ferrocene.

The electronic spectra of **1** and **2**, along with their oxidized counterparts $\mathbf{1}^+$ and $\mathbf{2}^+$, were studied by UV/Vis and EPR spectroscopy in CH_2Cl_2 (Figure 3). Absorption bands that are associated with π–π* and N–Fe ligand-to-metal charge-transfer (LMCT) processes were detected at 285 nm ($\varepsilon = 10000$–20000 $M^{-1}cm^{-1}$) and 310–340 nm (5000-10000 $M^{-1}cm^{-1}$), respectively. More relevant, the phenolate-to-metal LMCT processes,[8,11] which involve in- and out-of-plane pro cesses such as $p\pi_{phenolate} \rightarrow d\sigma^*_{Fe}$ and $p\pi_{phenolate} \rightarrow d\pi^*_{Fe}$, among others, appear between 420 and 500 nm (5800 and 3500 $M^{-1}cm^{-1}$, respectively) for **1**, and as a single broad band at around 480 nm (ca. 3300 $M^{-1}cm^{-1}$) for **2**. Bulk electrolysis of **1** and **2** at −78 °C with $TBAPF_6$ resulted in the singly oxidized species $\mathbf{1}^+$ and $\mathbf{2}^+$ with a remarkable decrease in the phenolate-to-iron LMCT processes. This decrease indicates that one of the phenolate groups has been transformed into a phenoxyl radical. The most remarkable feature of the electrolysis is

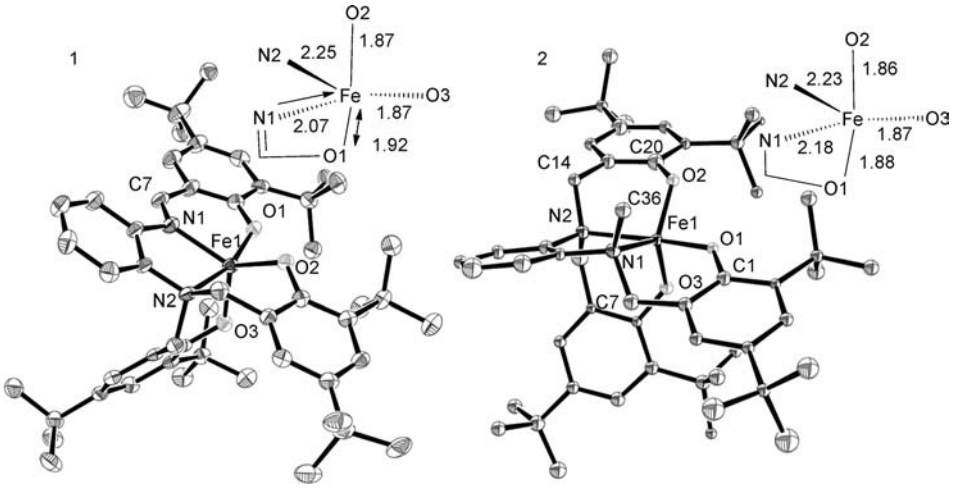

Figure 1. ORTEP diagrams for **1** and **2**. Bond lengths for **1** (left): Fe–O = ca. 1.89, Fe–N1 = 2.072(2), Fe–N2 = 2.24(2), C7–N1 = 1.32(3) Å. Bond lengths for **2** (right): Fe–O = ca. 1.87, Fe–N1 = 2.177(2), Fe–N2 = 2.234(2), C7–N1 = 1.512(3) Å.

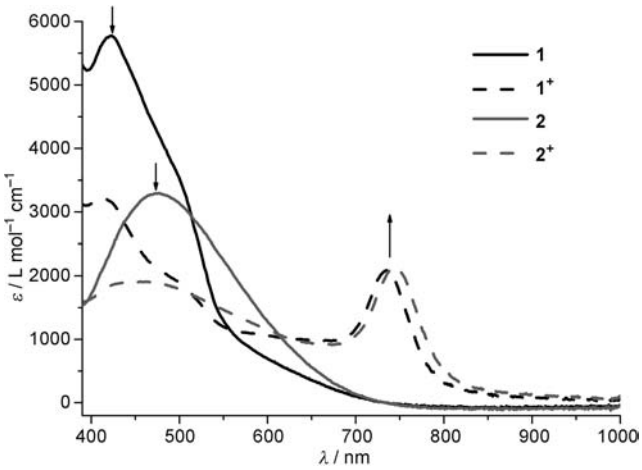

Figure 3. Electronic spectra for **1**, 1^+, **2**, and 2^+.

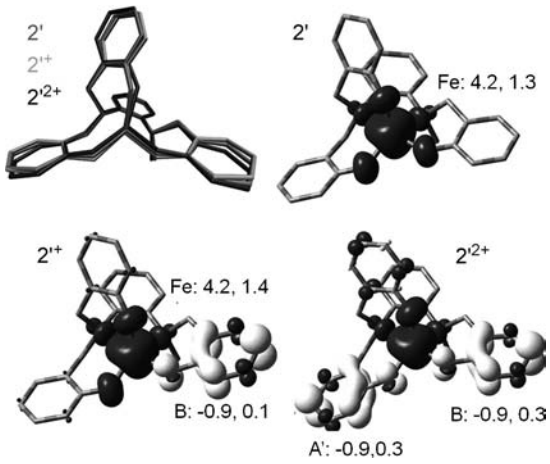

Figure 4. Structure overlap and spin density plot for **2′**, $\mathbf{2'}^+$, and $\mathbf{2'}^{2+}$. Values given after the atom or group labels are the charge and spin, respectively.

a new absorption band at approximately 750 nm for both $\mathbf{1}^+$ and $\mathbf{2}^+$. This band is attributed to the phenolate-to-phenoxyl interligand charge-transfer process. Previous studies on copper and nickel salen-type systems have shown that this band is located in the near-IR region at a considerably lower energy and intensity than would be expected for delocalized systems.[3d,12] The displacement of these bands to higher energies seems to be associated with one or more of the following: the localized nature of the charge-transfer process, the relative angle between the donor and the acceptor, and the energy of the resulting MOs that are involved with the charge-transfer process. As shown below, localization of the charge transfer seems to be dominant, which agrees well with recent results published by Stack and co-workers.[13]

The EPR spectra for **1** and **2** both have signals at $g = 4.3$, which is diagnostic of a five-coordinate, high-spin iron(III) ion in a largely anisotropic ligand field (Figures S1 and S2 in the Supporting Information). Upon ligand oxidation, this signal decreases in intensity by approximately 90% (calculated by the decrease in the area of the integrated curve), which is consistent with the existence of an antiferromagnetically coupled [$Fe^{III}L^{\bullet}$] species with an integer spin $S = [5/2-1/2] = 4/2$. Concomitantly, a new signal at $g = 2.0$ appeared and is associated with approximately 5% of a different species that has an uncoupled radical. These results also agree well with previous data.[3e,6b,c,8,14]

Electronic structure calculations were carried out on the models **1′** and **2′**, in which the *tert*-butyl groups were replaced by hydrogen atoms (Table S4 in the Supporting Information). The products of the sequential oxidations $\mathbf{1'} \rightarrow \mathbf{1'}^+ \rightarrow \mathbf{1'}^{2+}$ and $\mathbf{2'} \rightarrow \mathbf{2'}^+ \rightarrow \mathbf{2'}^{2+}$ were investigated. Based on available experimental evidence,[3e,6b,c,8,14] an antiferromagnetic coupling between the iron(III) center and the phenoxyl radicals was assumed. Figure 4 shows the structural changes and spin plots for species **2′**, its monocation $\mathbf{2'}^+$, and dication $\mathbf{2'}^{++}$. Only minor distortions were observed upon oxidation. Likewise, a consistent electronic density was calculated for the high-spin iron(III) ion. Comparable results were obtained for **1′** and its corresponding oxidation products (Figures S3 and S4 in the Supporting Information). The amount of spin density and the charges that are related to each phenolate/phenoxyl ring can be quantified by adding the contributions of the ring atoms together (Tables S5 and S6 in the Supporting Information). The phenolate rings for **1′** and **2′** exhibit Mulliken spin densities of 0.17–0.24 and charges of −0.3–−0.4. In contrast the monocation $\mathbf{1'}^+$ has an excess of β density. This excess is consistent with a phenoxyl radical on ring A that has a calculated spin density of −0.88 and charge of 0.20. Indeed, in the equivalent structure the Fe−OA′ bond is lengthened by approximately 0.11 Å and the C=O bond is shortened by 0.06 Å. These values suggest that the ring becomes quinoid-like in nature and less effective as an electron donor. As a consequence, the Fe−O bonds to both of the remaining phenolate rings A′ and B shorten. Model $\mathbf{1'}^{2+}$ behaves in a similar manner and a second phenolate-to-phenoxyl conversion takes place on ring A′. The relative absence of geometric rearrangements fosters the overall redox bistability that is required for fast redox cycling between these species.

Species $\mathbf{2'}^+$ behaves differently to species $\mathbf{1'}^+$ upon oxidation. The first oxidation leads to the formation of a phenoxyl radical on ring B. This is in clear opposition to the oxidation of ring A in **1′**. The phenolate of ring B is associated with the methyl-substituted nitrogen atom and has Mulliken spin density and charge of −0.92 and 0.13, respectively. The Fe−O bond is elongated by 0.13 Å and the C=O bond is shortened to 1.28 Å. These changes are in excellent agreement with the values observed for the quinoid-like structure of $\mathbf{1'}^+$. The values that were calculated for $\mathbf{2'}^{2+}$ also agree with the general trends that were discussed above for $\mathbf{1'}^{2+}$. It seems apparent that the nature of the nitrogen atoms (as a tertiary amine or an azomethine) leads to subtle but significant changes in the phenolate rings. The more π-acidic imino group stabilizes the phenolate-based HOMO that becomes less oxidizable than the equivalent aminophenolates. This change drives the electrochemical specificity of **1** and **2**. To our knowledge, this effect has not been reported for iron phenolate complexes before.

The analysis of MOs in high-spin species with $S = 5/2$ that are antiferromagnetically coupled to $S = 1/2$ organic radicals is far from trivial. In this study it was achieved by furthering

the approach of corresponding biorthogonal orbitals that was used by Neese to analyze magnetic coupling in coordination complexes,[15] in which the energies of the corresponding α and β orbitals are averaged to construct a classical MO ladder diagram. This approach was expanded to allow a qualitative energy ladder to be built (Table S7 in the Supporting Information). An increase in the charge for both complexes leads to a typical decrease in the relative energies of all of the frontier orbitals. This change indicates an increase in the ionization potential of the complexes that is related to a larger positive charge. Figure 5 depicts this diagram with arbitrarily assigned d orbitals for **2′** as $d_{xz} \geq d_{xy} > d_{x^2-y^2} > d_{yz} > d_{z^2}$. The first doubly occupied MO relates to the electrochemical processes that correspond to the oxidation of the phenolate phenoxyl radical, and accurately portrays the primary locus of the radical in $\mathbf{2'}^{+}$. Similarly, for $\mathbf{2'}^{+}$ the first doubly occupied MO relates to the second oxidative process. Interestingly, the presence of the azomethine group in complex **1′** leads to a shorter Fe–N1 bond and a longer Fe–O1 bond. This geometry affects the iron-based, singly occupied MO that coincides with the N1–Fe–O1 plane, and has an increased energy because of a π-antibonding interaction. The series $\mathbf{1'} \rightarrow \mathbf{1'}^{+} \rightarrow \mathbf{1'}^{++}$ has comparable oxidation behavior, however, the elongation of the Fe–O1 bond results in a reduction in the energy of the remaining four 3d orbitals (Figures S5–S7 in the Supporting Information). These calculations required the use of the IEF-PCM solvation model for the first doubly occupied MOs. Without solvation, the resulting radicals become delocalized over the three phenolate groups and lack physical meaning (Table S6 in the Supporting Information). As recently observed by Klüfers and co-workers[16] in square planar high-spin Fe^{II} species, it seems that five-coordination and low local symmetries around the metal ion support the formation of unique, highly nondegenerate MOs that are considerably distinct from an idealized $t_{2g}{}^{*}e_{g}{}^{*}$ octahedral scheme. These MOs rearrange in terms of energy upon ligand oxidation, which lowers the HOMOs, stabilizes the radicals, and allows redox cycling.

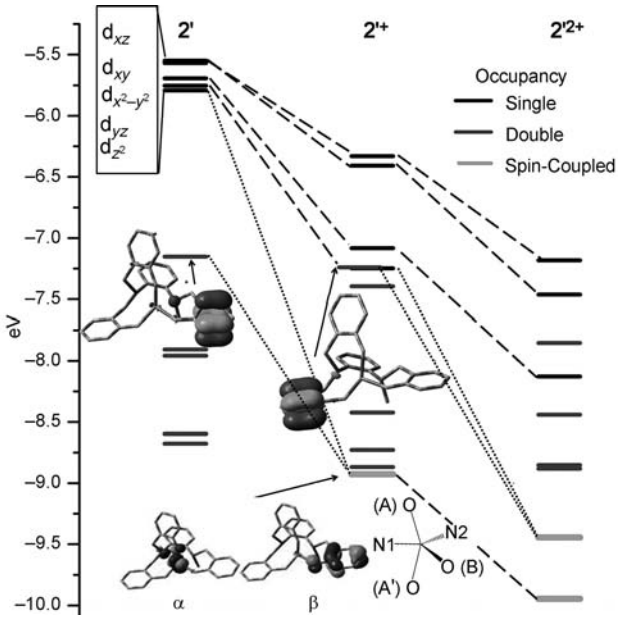

Figure 5. MO ladder for **2**, $\mathbf{2}^{+}$, and $\mathbf{2}^{2+}$.

In conclusion, two iron(III) complexes that incorporate the basic geometrical principles that are found in enzymes that form and cycle radicals were synthesized. Both species were formed with pentadentate N_2O_3 ligands that confer a low symmetry on the metal ion. To understand how five-coordination may influence their electronic and redox properties, these complexes were examined by experimental and theoretical methods. Subtle structural changes in the ligand, such as the introduction of a methyl group to the bridging nitrogen atom or the presence of an azomethyne group, are sufficient to change the oxidation sequence of the phenolate groups. This finding was corroborated by computational calculations and allowed individual redox loci to be assigned for each of these compounds and the corresponding oxidized species. Whether multiple, ligand-based oxidations occur in a consecutive or concerted fashion depends on the nature of the supporting electrolyte. We also found that these phenolate-rich, five-coordinate environments with nondegenerate orbitals seem to be amenable to redox cycling, as minimal decomposition was detected after 30 cycles. Spectroscopic changes that result from these sequential oxidations lead to a localized phenolate-to-phenoxyl charge-transfer process (Figure S8 in the Supporting Information). These results allow us to move one step further towards the development of redox-active molecular materials. Redox systems with alkoxy chains that are appended onto the phenylene ring are currently under development with the aim of merging redox properties with amphiphilic behavior and film deposition.

Experimental Section

Materials were used as received. Solvents were distilled before use. Infrared spectra were measured from 4000 to 400 cm^{-1} in KBr pellets on a Tensor 27 FTIR-Spectrophotometer. ^{1}H NMR spectra were measured on Varian 300 MHz and 400 MHz instruments. ESI^{+} spectra were measured in a triple-quadrupole Micromass Quattro LC spectrometer with an electrospray/atmospheric pressure chemical ionization (APCI) source. Experimental assignments were based on simulations of peak position and isotopic distributions. Elemental analyses were performed by Midwest Microlab, Indianapolis, IN. Cyclic voltammetry was performed on a Bioanalytcal Systems CV-50 W system. A standard Ag/AgCl, Pt-wire, vitreous C cell was used. The Fc/Fc^{+} couple (0.45 V in CH_2Cl_2)[17] was used as internal reference. Bulk electrolysis was performed in a vitreous carbon basket. The concentrations of the analytes were 1.0×10^{-3} M, and all supporting electrolytes were 0.1 M. First-derivative X-band EPR spectra in dichloromethane were obtained on a Bruker EXP 300 spectrometer at 125 K with liquid nitrogen as the coolant.

Molecular modeling: Spin-unrestricted DFT calculations were carried out with the B3LYP[18] functional and the 6-31G(d)[19] basis set in the development version of Gaussian.[20] Solvation in CH_2Cl_2 was modeled with the integral equation formalism polarizable continuum model (IEF-PCM).[21] Geometries were optimized without symmetry constraints, and stationary points were verified by frequency analysis. MO analysis was performed by using biorthogonal corresponding orbital approaches;[15] the energies were obtained by a unitary transformation of the unrestricted Fock matrices into the biorthogonal basis. The average of the energies of the α and β biorthogonalized orbitals were computed and used to approximate the energies

of the restricted MOs. These MO energies were then used to build a classical restricted MO diagram (Figures S6 and S7 in the Supporting Information). Cartesian coordinates of all optimized structures are provided in the Supporting Information.

Syntheses: The ligands H_3L^1 and H_3L^2 were synthesized as reported.[6b,c] [FeL^1] (**1**) and [FeL^2] (**2**) were obtained as follows: a solution of the ligand (1 equiv) in CH_2Cl_2 was treated with a solution of iron(III) chloride (1 equiv) in warm methanol, in the presence of $NaOCH_3$ (3 equiv) at 50 °C for 30 min in an inert atmosphere. The reaction continued under aerobic conditions for a further 1 h. The solvent was then removed by rotary evaporation and the crude, dark reddish-brown powder was recrystallized from $MeOH/CH_2Cl_2$ (1:2), to yield single crystals that were suitable for analysis by X-ray diffraction. [FeL^1] (**1**): Yield: 60%. ESI$^+$ (m/z) = 814.4, 100% for $[C_{51}H_{69}N_2O_3Fe+H]^+$. Elemental analysis calcd (%) for $C_{51}H_{69}N_2O_3Fe$: C 75.26, H 8.54, N 3.44; found: C 75.24, H 8.81, N 3.45. IR (KBr): $\tilde{\nu}$ = 2956(s), 2870(s), (C–H, alkane); 1611(s), (C=N); 1470(s), 1445(s), (C=C aryl); 1199(s), (C–O); 873 cm^{-1} (s), (C–H, phen). [FeL^2] (**2**): Yield: 65%. ESI$^+$ (m/z, in MeOH) = 830.9, 100% for $[C_{52}H_{73}N_2O_3Fe+H]^+$. Elemental analysis calcd (%) for $C_{52}H_{73}N_2O_3Fe+H$: C 75.25, H 8.86, N 3.38; found: C 74.97, H 8.80, N 3.28. IR (KBr): $\tilde{\nu}$ = 2955(s), 2909(s), 2872(s), (C–H, alkane); 1274(s), (C–N); 1481(s), 1445(s), 851 cm^{-1} (s), (C–H, phen).

X-ray diffraction: Data were collected on a Bruker APEX-II Kappa geometry diffractometer with Mo radiation and a graphite monochromator at 100 K. **1**: 29085 reflections collected; 10851 unique; no associated solvates. One *tert*-butyl group required the assignment of partial occupancies. **2**: 49239 reflections collected; 11772 unique, only 4089 had $I > 2\sigma(I)$. The small red needles diffracted poorly. Data was integrated with SMART, SAINT, and SADABS[22] software. Refinement used SHELX-97[23] software. Crystal structure parameters for all structures are listed in Tables S1 and S2 in the Supporting Information.

Received: May 11, 2011
Revised: November 9, 2011
Published online: December 12, 2011

Keywords: electronic structure · iron · oxidation · radicals · redox chemistry

[1] a) O. Sato, J. Tao, Y.-Z. Zhang, *Angew. Chem.* **2007**, *119*, 2200 – 2236; *Angew. Chem. Int. Ed.* **2007**, *46*, 2152 – 2187; b) O. Kahn, *Acc. Chem. Res.* **2000**, *33*, 647 – 657.

[2] a) E. R. Kay, D. A. Leigh, F. Zerbetto, *Angew. Chem.* **2007**, *119*, 72 – 196; *Angew. Chem. Int. Ed.* **2007**, *46*, 72 – 191; b) S. Flores-Torres, G. R. Hutchison, L. J. Soltzberg, H. D. Abruña, *J. Am. Chem. Soc.* **2006**, *128*, 1513 – 1522; c) A. Dei, D. Gatteschi, C. Sangregorio, L. Sorace, *Acc. Chem. Res.* **2004**, *37*, 827 – 835; d) R. A. Wassel, C. B. Gorman, *Angew. Chem.* **2004**, *116*, 5230 – 5233; *Angew. Chem. Int. Ed.* **2004**, *43*, 5120 – 5123; e) J. Park, A. N. Pasupathy, J. I. Goldsmith, C. Chang, Y. Yaish, J. R. Petta, M. Rinkoski, J. P. Sethna, H. D. Abruna, P. L. McEuen, D. C. Ralph, *Nature* **2002**, *417*, 722 – 725; f) L. Fabbrizzi, M. Licchelli, P. Pallavicini, *Acc. Chem. Res.* **1999**, *32*, 846 – 853; g) O. Kahn, C. J. Martinez, *Science* **1998**, *279*, 44 – 48.

[3] a) M. Orio, O. Jarjayes, H. Kanso, C. Philouze, F. Neese, F. Thomas, *Angew. Chem.* **2010**, *122*, 5109 – 5112; *Angew. Chem. Int. Ed.* **2010**, *49*, 4989 – 4992; b) Y. Shimazaki, T. D. P. Stack, T. Storr, *Inorg. Chem.* **2009**, *48*, 8383 – 8392; c) L. H. Tong, Y.-L. Wong, S. I. Pascu, J. R. Dilworth, *Dalton Trans.* **2008**, 4784 – 4791; d) T. Storr, E. Wasinger, R. Pratt, T. Stack, *Angew. Chem.* **2007**, *119*, 5290 – 5293; *Angew. Chem. Int. Ed.* **2007**, *46*, 5198 – 5201; e) C. Imbert, H. P. Hratchian, M. Lanznaster, M. J. Heeg, L. M. Hryhorczuk, B. R. McGarvey, H. B. Schlegel, C. N. Verani, *Inorg. Chem.* **2005**, *44*, 7414 – 7422; f) L. Benisvy, A. J. Blake, D. Collison, E. S. Davies, C. D. Garner, E. J. L. McInnes, J. McMaster, G. Whittaker, C. Wilson, *Chem. Commun.* **2001**, 1824 – 1825; g) M. D. Snodin, L. Ould-Moussa, U. Wallmann, S. Lecomte, V. Bachler, E. Bill, H. Hummel, T. Weyhermüller, P. Hildebrandt, K. Wieghardt, *Chem. Eur. J.* **1999**, *5*, 2554 – 2565; h) B. Adam, E. Bill, E. Bothe, B. Goerdt, G. Haselhorst, K. Hildenbrand, A. Sokolowski, S. Steenken, T. Weyhermüller, K. Wieghardt, *Chem. Eur. J.* **1997**, *3*, 308 – 319; i) A. K. Nairn, R. Bhalla, S. P. Foxon, X. Liu, L. J. Yellowlees, B. C. Gilbert, P. H. Walton, *Dalton Trans.* **2002**, 1253 – 1255.

[4] A. J. Ramsey, P. J. Hillas, P. F. Fitzpatrick, *J. Biol. Chem.* **1996**, *271*, 24395 – 24400.

[5] a) M. Y. M. Pau, M. I. Davis, A. M. Orville, J. D. Lipscomb, E. I. Solomon, *J. Am. Chem. Soc.* **2007**, *129*, 1944 – 1958; b) T. Borowski, P. E. M. Siegbahn, *J. Am. Chem. Soc.* **2006**, *128*, 12941 – 12953; c) M. Ferraroni, J. Seifert, V. M. Travkin, M. Thiel, S. Kaschabek, A. Scozzafava, L. Golovleva, M. Schloemann, F. Briganti, *J. Biol. Chem.* **2005**, *280*, 21144 – 21154.

[6] a) F. D. Lesh, R. Shanmugam, M. M. Allard, M. C. Lanznaster, M. J. Heeg, M. T. Rodgers, J. M. Shearer, C. N. Verani, *Inorg. Chem.* **2010**, *49*, 7226 – 7228; b) M. Lanznaster, M. J. Heeg, G. T. Yee, B. R. McGarvey, C. N. Verani, *Inorg. Chem.* **2007**, *46*, 72 – 78; c) M. Lanznaster, H. P. Hratchian, M. J. Heeg, L. M. Hryhorczuk, B. R. McGarvey, H. B. Schlegel, C. N. Verani, *Inorg. Chem.* **2006**, *45*, 955 – 957.

[7] a) P. J. Chirik, K. Wieghardt, *Science* **2010**, *327*, 794 – 795; b) P. Chaudhuri, C. N. Verani, E. Bill, E. Bothe, T. Weyhermüller, K. Wieghardt, *J Am Chem. Soc* **2001**, *123*, 2213 – 2223.

[8] T. Kurahashi, Y. Kobayashi, S. Nagatomo, T. Tosha, T. Kitagawa, H. Fujii, *Inorg. Chem.* **2005**, *44*, 8156 – 8166.

[9] R. L. Lintvedt, L. S. Kramer, *Inorg. Chem.* **1983**, *22*, 796 – 802.

[10] a) W. E. Geiger, F. D. R. Barrière, *Acc. Chem. Res.* **2010**, *43*, 1030 – 1039; b) F. Barrière, W. E. Geiger, *J. Am. Chem. Soc.* **2006**, *128*, 3980 – 3989; c) A. Nafady, T. T. Chin, W. E. Geiger, *Organometallics* **2006**, *25*, 1654 – 1663.

[11] M. I. Davis, A. M. Orville, F. Neese, J. M. Zaleski, J. D. Lipscomb, E. I. Solomon, *J. Am. Chem. Soc.* **2002**, *124*, 602 – 614.

[12] a) T. Storr, P. Verma, R. C. Pratt, E. C. Wasinger, Y. Shimazaki, T. D. P. Stack, *J. Am. Chem. Soc.* **2008**, *130*, 15448 – 15459.

[13] T. Storr, P. Verma, Y. Shimazaki, E. C. Wasinger, T. D. P. Stack, *Chem. Eur. J.* **2010**, *16*, 8980 – 8983.

[14] T. Kurahashi, H. Fujii, *J. Am. Chem. Soc.* **2011**, *133*, 8307 – 8316.

[15] F. Neese, *J. Phys. Chem. Solids* **2004**, *65*, 781 – 785.

[16] X. Wurzenberger, H. Piotrowski, P. Klüfers, *Angew. Chem.* **2011**, *123*, 5078 – 5082; *Angew. Chem. Int. Ed.* **2011**, *50*, 4974 – 4978.

[17] R. R. Gagne, C. A. Koval, G. C. Lisensky, *Inorg. Chem.* **1980**, *19*, 2854 – 2855.

[18] a) A. D. Becke, *J. Chem. Phys.* **1993**, *98*, 5648 – 5652; b) B. Miehlich, A. Savin, H. Stoll, H. Preuss, *Chem. Phys. Lett.* **1989**, *157*, 200 – 206; c) C. Lee, W. Yang, R. G. Parr, *Phys. Rev. B* **1988**, *37*, 785 – 789.

[19] a) V. A. Rassolov, M. A. Ratner, J. A. Pople, P. C. Redfern, L. A. Curtiss, *J. Comput. Chem.* **2001**, *22*, 976 – 984; b) V. A. Rassolov, J. A. Pople, M. A. Ratner, T. L. Windus, *J. Chem. Phys.* **1998**, *109*, 1223 – 1229; c) R. Ditchfield, W. J. Hehre, J. A. Pople, *J. Chem. Phys.* **1971**, *54*, 724 – 728.

[20] M. J. Frisch, Revision H.04 ed., Gaussian, Inc. (see Supporting Information for full citation), Wallingford, CT, **2009**.

[21] a) J. Tomasi, B. Mennucci, R. Cammi, *Chem. Rev.* **2005**, *105*, 2999 – 3094; b) S. Miertuš, J. Tomasi, *Chem. Phys.* **1982**, *65*, 239 – 245; c) S. Miertuš, E. Scrocco, J. Tomasi, *Chem. Phys.* **1981**, *55*, 117 – 129.

[22] SMART, SAINT, and SADABS collection and processing programs are distributed by the manufacturer, Bruker AXS, Inc., Madison, WI, USA, 2001.

[23] G. Sheldrick, *Acta Crystallogr. Sect. A* **2008**, *64*, 112 – 122.

